PNNL-22194

Prepared for the U.S. Department of Energy
under Contract DE-AC05-76RL01830

Modeling and Simulation Capabilities for the Evaluation of Micro Grids

KP Schneider
FK Tuffner
MA Elizondo
A Somani
B Vyakaranam
JC Fuller
D Wu
MJ Rice
AR Fisher

January 2013

PACIFIC NORTHWEST NATIONAL LABORATORY

operated by

BATTELLE

for the

UNITED STATES DEPARTMENT OF ENERGY

under Contract DE-AC05-76RL01830

Printed in the United States of America

Available to DOE and DOE contractors from the Office of Scientific and Technical Information,

P.O. Box 62, Oak Ridge, TN 37831-0062; ph: (865) 576-8401 fax: (865) 576-5728 email: reports@adonis.osti.gov

Available to the public from the National Technical Information Service,

U.S. Department of Commerce, 5285 Port Royal Rd., Springfield, VA 22161

ph: (800) 553-6847 fax: (703) 605-6900

email: orders@ntis.fedworld.gov online ordering: http://www.ntis.gov/ordering.htm

 This document was printed on recycled paper.

(1/2013)

Modeling and Simulation Capabilities for the Evaluation of Micro Grids

KP Schneider
JC Fuller
FK Tuffner
D Wu
MA Elizondo
MJ Rice
A Somani
AR Fisher
B Vyakaranam

January 2013

Prepared for
the U.S. Department of Energy
under Contract DE-AC05-76RL01830

Pacific Northwest National Laboratory
Richland, Washington 99352

Table of Contents

Table of Figures

Table of Tables

Summary

Micro grids are a potential solution to the goals of increasing the reliability and the efficiency of electric power systems while at the same time reducing emissions. As with the majority of power system technologies, achieving these goals in a cost effective manner requires simulation and analysis. Unfortunately, the analysis of micro grids is limited by the tools that are commercially available. The planning and operational tools commonly used by power system engineers today were designed for the analysis of traditional grid connected power systems, not micro grids. To help address the lack of openly available simulation and analysis capabilities for micro grids, the Department of Energy's Office of Electricity Delivery and Energy Reliability (DOE-OE) has developed an active research area in micro grids. As part of the DOE-OE micro grid research program, the Pacific Northwest National Laboratory (PNNL) is developing fundamental simulation and analysis capabilities in an open source environment. This report details the development of simulation and analysis capabilities for micro grids in the GridLAB-D™ simulation environment.

1 Introduction

Micro grids have been deployed around the world because of their ability to provide electricity in urban and remote locations with exceptionally high levels of reliability. One of the reasons that micro grids are able to provide high levels of reliability is that the generation sources are located near the end-use loads and they are not reliant on a large interconnected transmission system. The generation sources in micro grids can be traditional units or a combination of traditional units and renewables units. In the United States, micro grids are primarily deployed to increase the reliability of high-value critical end-use loads; the average residential customer is not supplied by a micro grid. This is due to the traditionally high cost of designing and operating micro grids, which is partially due to the lack of effective simulation and analysis tools.

As part of the DOE-OE agenda, there are program level goals for both smart grid and micro grids, both have target dates of 2020. The micro grid analysis efforts of DOE-OE are a subset of the smart grid program. Table 1.1 and Table 1.2 show the smart grid and micro grid program goals for DOE-OE.

Table 1.1: DOE-OE smart grid goals for 2020

Smart Grid (2020)	
Goal 1	20% reduction in SAIDI
Goal 2	20% reduction in load factor
Goal 3	>98% reduction in outages

Table 1.2: DOE-OE micro grid goals for 2020

Micro Grid (2020)	
Goal 1	Cost parity with DGs and UPSs
Goal 2	20% improvement in efficiency
Goal 3	>98% reduction in outages
Goal 4	>20% reduction of emissions

To support the DOE-OE goals for micro grid, and parent smart grid, programs in Fiscal Year (FY) 12, PNNL developed two key simulation and analysis capabilities in the open source simulation environment GridLAB-D. The first was the ability to conduct transient-level dynamic simulations of unbalanced distribution systems, and micro grids. This first capability will help to make micro grids more cost effective by allowing a more accurate design that does not require conservatively oversized equipment. The second is the ability to implement multi-objective controls in an open-source framework. This second capability will help to make micro grids more cost effective through optimization of resources, which will also lead to higher efficiencies and reduce emissions. Both of the developed capabilities were tested using a model of the Oak Ridge National Laboratories (ORNL) Distributed Energy Communications & Controls (DECC) test facility.

This document is organized as follows. Section 2 outlines the specific capabilities of the transient-level dynamic simulation that were developed and Section 3 outlines the specific capabilities of multi-objective controls that were developed. Section 4 contains the concluding remarks.

2 Dynamic Simulations for Micro Grids

Micro grids are currently deployed primarily to provide high reliability power to critical or remote end-use loads. Often, this is in the context of better power quality generation or backup generation for continuous operation. At this time, the deployment of micro grids is limited, primarily due to the costs of design, construction, and operation. Without the required simulation capability, it is difficult to develop a robust design, which impacts operational efficiencies.

As part of the FY12 GridLAB-D tasks, the basic capability to perform transient-level simulations of a microgrid environment with timesteps of approximately 1 millisecond or greater were introduced. Utilizing the open-source framework of GridLAB-D, this capability will allow the exploration of micro gird designs and deployments, along with their potential benefits on a larger scale.

2.1 Capabilities

The micro grid capabilities included in GridLAB-D for the FY12 efforts are a solid foundation, but they do not represent all necessary capabilities. The basic framework for powerflow studies and simulation of new technologies was developed, along with an initial synchronous machine model. This framework supports the normal GridLAB-D capability of time-series simulations of many objects, including playing field measured data into the simulation.

The most significant capability developed is the ability to simulate the transient dynamics of an unbalanced distribution system. Many simulation software tools support the transient simulation of balanced systems, typically associated with transmission-level studies. Micro grids are typically much smaller systems and operate in conditions similar to distribution-level power systems. The unbalanced nature of the distribution system makes the traditional transmission-level transient dynamics approach insufficient. GridLAB-D implements the transient behaviors in a manner that supports the unbalanced conditions present in a typical distribution network. Factoring in these additional effects allows a much more accurate representation of the electric grid-level concerns operating a micro grid may produce. The transient simulation capabilities developed are applicable to unbalanced distribution systems as well as micro grids.

As a first step, a simple synchronous diesel generator model was implemented inside GridLAB-D. The synchronous diesel generator model allows initial investigations into microgrid behavior. Many traditional micro grid scenarios are built on some form of fossil-fueled synchronous generator, so the diesel generator provides a good starting point for analysis. It also provides a basic framework for additional devices planned for FY13 development, such as inverters and synchronous condensers.

2.2 Implementation

The transient simulation capability for micro grid simulations is implemented in two basic parts: super-second and sub-second. The default mode, super-second, allows GridLAB-D to simulate at 1-second or longer time steps. These time steps are driven by state changes, so if no

change occurs for 1 day, GridLAB-D advances the simulation time by 1 day. GridLAB-D is often used to perform year-long simulations of test systems, so the ability to implement a variable time step has proven to reduce simulation run times.

Simulating a full year at 1-milisecond time steps would result in significant computation time. However, there are simulation periods where this level of detail is needed. Similar to the super-second implementation, GridLAB-D has the ability to change time step increments into sub-second values, and then return to super-second values. Specifically, the simulation can move along at 1-minute intervals, enter sub-second for two minutes of simulation time at 1-millisecond time steps, and then return to the 1-minute time step afterwards. This allows it to capture the dynamic capabilities during those two minutes, but still progress through the simulation interval at a reasonable pace.

To perform this mixed mode of simulation, GridLAB-D controls various "transient dynamic" aspects of the system at the super-second level. When a transient event occurs, it will enter sub-second resolution until the transient-level simulation stabilizes at a new operating point, and then return to super-second simulation. The details of these two modes are detailed in the following sections.

2.2.1 Super-second simulation

The super second simulation is the quasi steady state values of the real and reactive power output of the generators in the micro grid. The real power output of the generators is based on load sharing using a simplified frequency droop control. The reactive power output of the generators will change VAR output for generators that are providing voltage regulation.

Frequency droop control is a control strategy that allows for multiple generators to respond to a system-wide change in load with no communication between the generators. The generators change their power output based on the changes in the frequency. As load increases, the system frequency decreases. Each generator has a slope for governor response as frequency deviates from nominal. For super-second simulation, a simplified frequency droop control scheme is implemented that proportionally adjusts each generator power output to the final, steady state frequency value. The explicit steps of the adjustment are detailed in the next paragraph.

The micro grid implementation in GridLAB-D models each of the three phases explicitly. Thus the modification of the frequency droop control had to be made to properly account for load changes on a per phase level. In the traditional positive sequence method, generation output is a single value which is the sum power the three phases. The steps in calculating real power output of each generator per phase are as follows:

1. Determine total system real power imbalance per phase and sum for all three phases.
2. Calculate the change in total output of the generator based on frequency droop response of the imbalance.

3. Calculate the change per phase per generator using the ratio of imbalance per phase over total system imbalance and total output change per generator.
4. Verify the generator is operating within limits.

The Automatic Voltage Regulation (AVR) control scheme changes the VAR output of the generator to maintain proper terminal voltage. Unlike many other devices in GridLAB-D, such as shunt capacitors, the AVR only controls its output; there is no remote bus control. The assumption was made that voltage regulation is performed per generator and not per phase. Thus the target voltage used in AVR is the positive sequence voltage of the terminal node. In typical power flow algorithms, generation buses with AVR enabled are transformed from PQ to PV in matrix calculations. In the GridLAB-D implementation of AVR, buses are still treated as PQ and change their VAR output as a secondary control (not modifying the matrices used in powerflow) to obtain the correct voltage at the bus. The algorithm enforces VAR limits and total MVA rating of the generator. This methodology more closely represents how generating units with voltage control capabilities operate.

These quasi steady state control strategies provide the response to changes in loads or loss in generation once the dynamics have occurred. Once the grid is operating at the new equilibrium found using frequency droop and AVR, then more advance system wide control strategies such as Multi-Objective control can be used.

2.2.2 Sub-second Transient Simulation

The GridLAB-D transient simulation model represents electro-mechanical dynamics of a micro grid with unbalanced loads and three-phase diesel distributed generators. The micro grid network is also fully represented and can have any level of phase unbalances (e.g. single phase laterals).

One of the main obstacles to overcome in the transient simulations was the representation of three phase generators symmetry built (symmetric geometric distribution of stator three-phase windings) in the micro grid network solution. Although [1] implements symmetry built constraint of the generator to a distribution network, the generators were modeled with pre-defined active and reactive power output, and the distribution network needed a connection to a larger power system. These two conditions are not met in isolated micro grids. In this work, an original solution was formulated to consider generator symmetry built in the network model of an isolated micro grid. This solution allows for adequate initialization of transient-level dynamic model from the super-second simulations or any other steady state condition.

The current transient simulation development includes the following models:

- Three phase sub-transient synchronous machine model that accounts for unbalanced loading as formulated in [2] and [3],
- Woodward diesel governor (DEGOV1) that modifies the mechanical power of the diesel generator to control the generator speed (and hence the system frequency),

- Simplified exciter system (SEXS) that modifies the generator field voltage (and hence its reactive power) to control the generator's terminal voltage (average voltage of each phase),
- Unbalanced distribution network model that accounts for the generator's symmetry build, extending the method of [4], and
- ZIP unbalanced load models.

Unbalanced operation of three phase synchronous machines is modeled using a simplified fundamental frequency model in phasor representation according to [2],[5]-[7]. This simplification allows representing the machine in symmetrical components where the positive sequence represents the main electrical torque, and the negative sequence current produces a torque in opposition. The total electrical torque is constant, facilitating the solution and determination of equilibrium. However, the variation of electrical torque due to unbalanced operation reported in [3], [8] is ignored. In addition, typical assumptions for transient stability models are also made: ignoring sub-transient saliency, and neglecting the stator dynamics [9].

Figure 2.1 summarizes the process for the GridLAB-D micro grid dynamic simulations. Details of the formulation and algorithms can be found in [10].

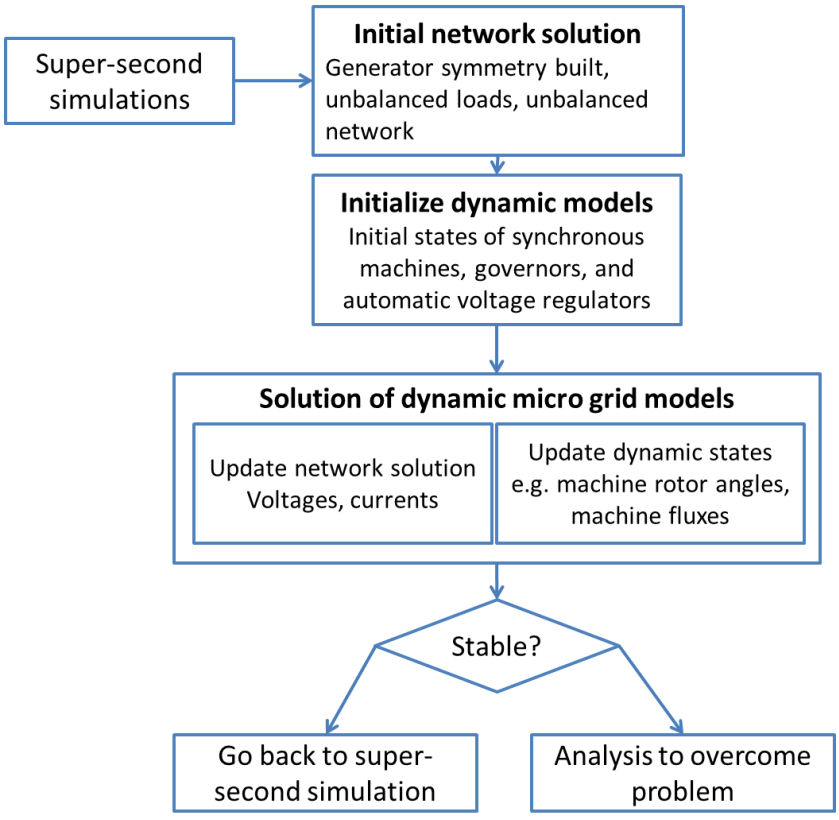

Figure 2.1: Micro grid transient simulations in GridLAB-D

2.3 Test Systems

With the basic micro grid capabilities within GridLAB-D, tests of the sub-second dynamics capability were necessary. Two systems were simulated as part of the validation effort for the FY12 GridLAB-D developments. The first system is a simple three-node system, while the second is a simplified version of Oak Ridge National Laboratory's Distributed Energy Communications and Control (DECC) facility. The details of the models and some simulation results are shown in the next subsection.

2.3.1 Three-Node System

The first system simulated was a basic three-node system. The system, shown in Figure 2.2, consists of two diesel generators (G1 and G2) and an unbalanced load (L1). The major generator parameters are provided in Table 2.1 below. There are many other parameters for the generators that are available in the test case under the GridLAB-D version 2.3 repository [11]. The system is extremely simple, but provides a method for testing network interactions and generator dynamics with a reasonable level of complexity. This verifies the underlying functionality of the micro grids capabilities, providing confidence for future studies that the recorded response is correct.

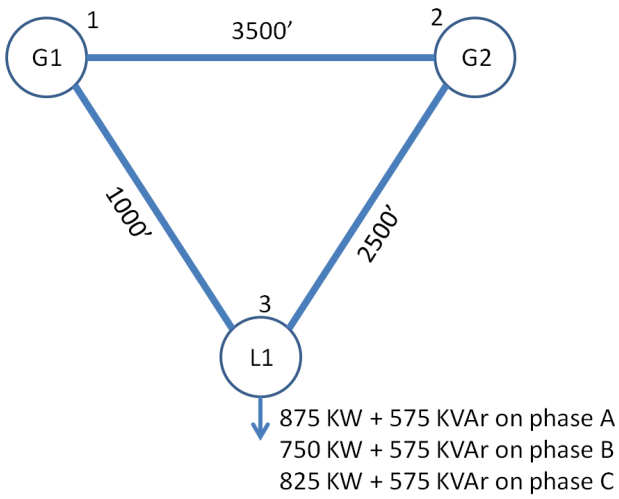

Figure 2.2: One-line diagram of simple three-node test system

Table 2.1: Parameters of implemented diesel generators

Diesel Generator Parameters	
Parameter	**Value**
Power	10 MVA
Voltage	15 kV
H	0.7 seconds
Ra	0.00625 p.u.
Xd	2.06 p.u.
Xq	2.5 p.u.
AVR	SEXS-type
GOV	DEGOV1-type

Upon constructing the test system of Figure 2.2, a simple dynamic event was simulated to verify the transient capabilities of GridLAB-D. For the fault, 10% of the load was shed instantaneously at the 5.0-second mark of the simulation. This would be similar to an under-frequency relay tripping a portion of the load, or a larger piece of equipment failing on the distribution feeder.

Figure 2.3 shows the GridLAB-D simulation results of the bus voltages for G1 and G2 of the simulated system with the 10% load shed. Figure 2.3 shows the rotor speeds for the same gernators during the same event. For this simple system, the AVR and GOV control objects quickly activate to stabilize the system within 30 seconds. The simulation then progresses back into standard GridLAB-D mode (super-second) and finishes the simulation. Further channels of data can be examined by running the example document from the GridLAB-D repository [11].

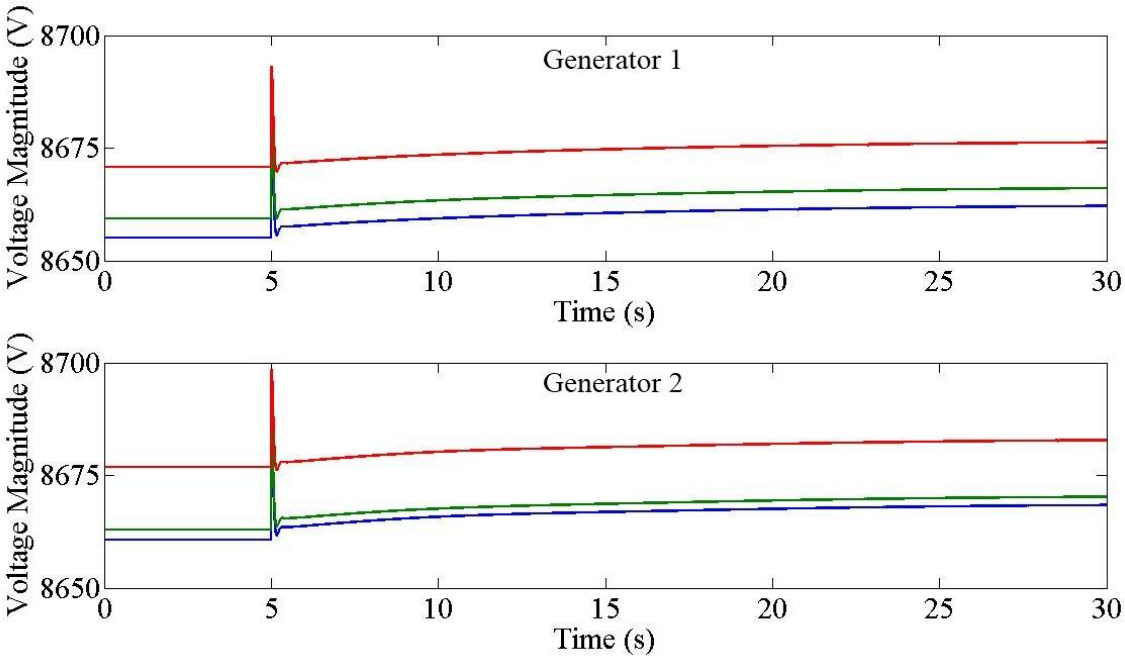

Figure 2.3: Simulated voltage response of simple three-node system to 10% load drop

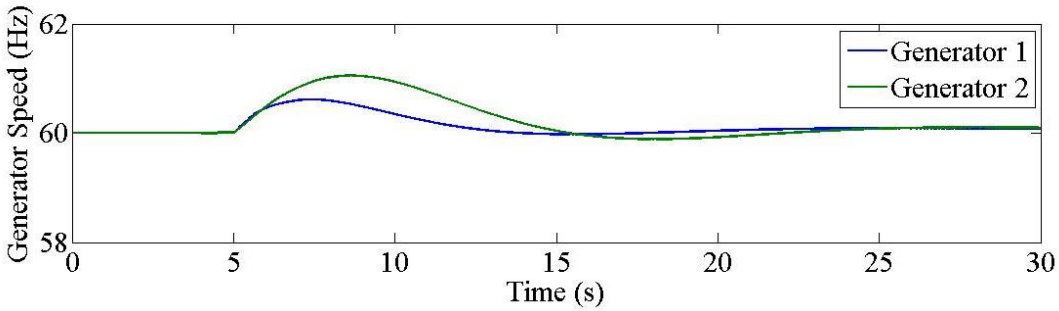

Figure 2.4. Simulated generator speed response of simple three-node system to 10% load drop

2.3.2 Modified DECC Facility Model

To provide a more realistic exercising of the initial GridLAB-D micro grid functionality, a more complicated model was constructed and simulated. Figure 2.5 shows the one-line diagram for a reduced-order model of the Oak Ridge National Laboratory DECC facility. The DECC facility is used to test equipment and evaluate micro grid operations of the equipment. The implementation of Figure 2.5 represents the topology of the DECC facility, but the actual equipment is completely fictional in this example. Loads and devices under test in the DECC facility are represented by time-varying loads within GridLAB-D. Two diesel generators with the base parameters of Table 2.1 are attached to the system to power the loads. To create a more interesting scenario, the generators were sized slightly different with G1 having a 500 KVA rating and G2 having a 250 KVA rating.

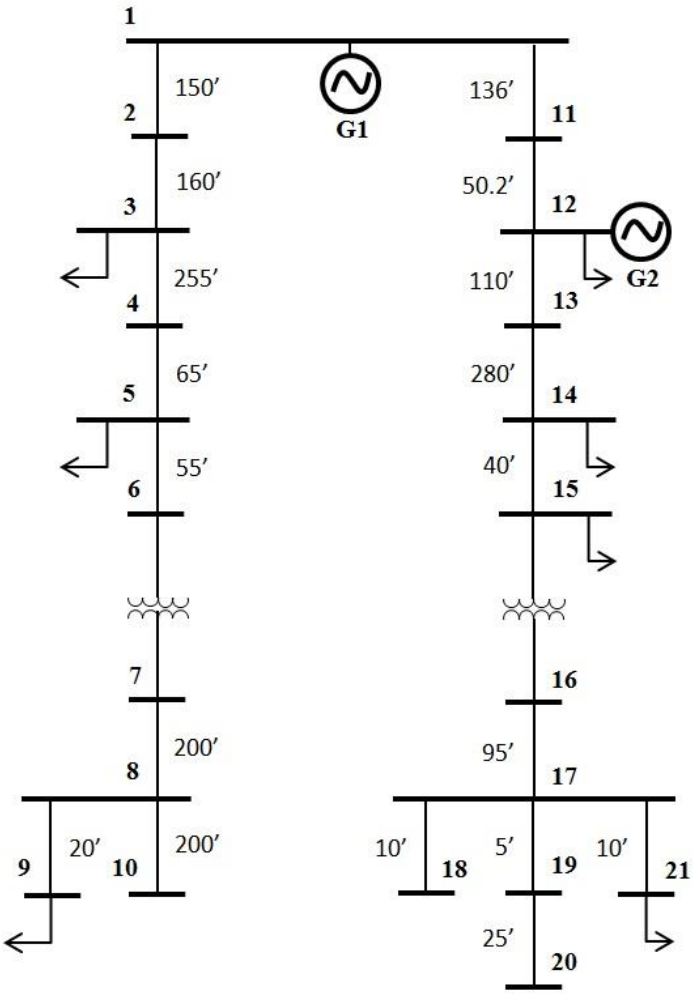

Figure 2.5: One-line diagram of simplified model of Oak Ridge National Laboratory DECC Facility

To provide a discrete event and excite the various dynamics of the system, the state of two loads on the DECC facility model were modified. From Figure 2.5, the load at bus 12 was completely removed and the load at bus 9 was double. These two changes occurred

simultaneously 10 seconds into the simulation. The results of this change on the rotational speeds of the two generators are shown in Figure 2.6. Figure 2.6 shows that a significant frequency deviation occurred. Such a load change is also expected to impact the rotor angle of the generaotrs, which is shown in figure 2.7. The rotor angle obviously goes through a significant adjustment, followed by a steady trend once the system stabilizes. The load at bus 12 represents about one-eighths of the total system peak load, so its sudden loss creates a significant shift in the powerflow of the system. The governors and exciters eventually activate and bring the system back to a stable operating point. If over frequency protection were in place, this large deviation could cause significant stability problems as more load tripped off the system. As such, being able to simulate such a large change in load is useful for investigating different strategies for mitigating the impact on the micro grid system.

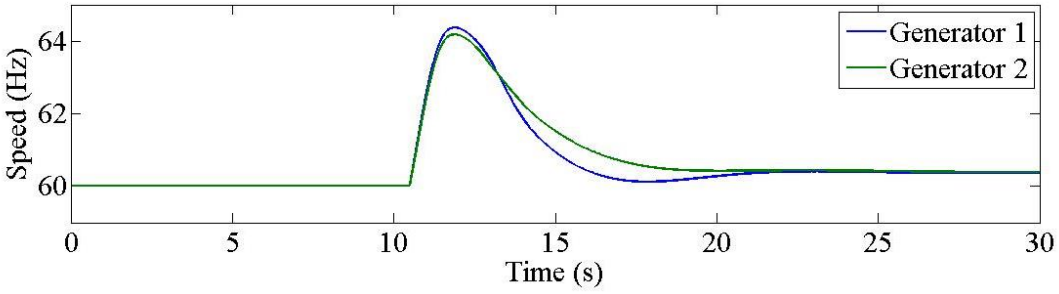

Figure 2.6: Simulated rotor speed of generators in simplified DECC model to a double load change

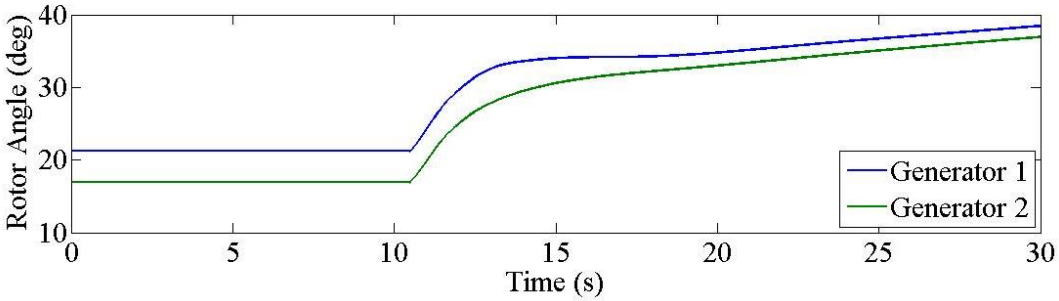

Figure 2.7. Simulated rotor angle of generators in simplified DECC facility to a double load change

The double load change of Figure 2.6 and Figure 2.7, along with the simple simulation of Figure 2.5 and Figure 2.5 show the initial implementation of unbalanced transient-level dynamics in GridLAB-D is working properly. GridLAB-D is modeling the explicit behavior of the unbalanced system on the diesel generators. More models are being developed in FY13 to provide greater system compatibility. However, the results shown here highlight the basic capability is within GridLAB-D to begin evaluating micro grid scenarios and conditions. This includes generator control strategies, and other approaches that could utilize the multi-objective control discussed in Section 3.

3 Multi-Objective Control

One of the most challenging aspects of emerging smart grid technologies is the formulation of an effective business case. Because of the need to modernize much of the existing infrastructure, the deployment of these technologies incurs a substantial capital cost. When the capital cost of deployment is compared to the benefits from a single application, such as peak shaving, it can often be difficult to make a convincing business case. This is especially true when deploying assets to support micro grids, as the business case for reliability improvements only is rather difficult to make. One option to address this issue is to use the deployed resource for multiple tasks, such as peak reduction and ramping services, by utilizing the same resource in different ways at different times, while reserving the capability for standalone operation in a micro grid for increased reliability. By using a control system that engages multiple benefit streams, the business case for emerging technologies becomes more favorable. While it is not possible to examine all of the possible combinations of benefit streams, the basic framework for testing and evaluating multi-objective controls was established.

This subtask focused on developing a control framework for multi-objective control of smart grid assets. Specific capabilities added to the GridLAB-D environment to support these activities are discussed in Section 3.1. A specific implementation is discussed in Section 3.2 using a dual-objective battery/inverter control case, while a test case utilizing the ORNL DECC facility model is discussed in Section 3.3.

3.1 Capabilities

Multi-objective control, often called multi-objective optimization, aims to simultaneously optimize for multiple objectives, while minimizing the global cost (or maximizing global utility) as defined by the optimization function. Often the objectives are conflicting, requiring a balance and trade-off between the different decision variables, while constraints are applied to a variety of decision variables. An example of a dual-objective control problem in power systems is energy storage being used for multiple energy or ancillary services, such as peak shaving and spinning reserve. Each service provides value, such as a payout from the wholesale energy provider, but also reduces the availability of the other service by consuming energy from the battery. By reducing the state of charge (SOC) during a peak shaving event, it limits the amount of capacity available for participation in a spinning reserve market. Ideally, the battery should operate in such a way that both objectives can be mostly achieved while obtaining maximum value for the two services over a pre-determined time horizon. Multi-objective controls attempt to weight these two functions in such a way as to maximize the profit of the battery by balancing each of the objectives in a coordinated manner.

There are a number of techniques for solving multi-objective optimization and control: integer programming, dynamic programming, heuristic techniques, genetic algorithms, particle swarm optimizers, tabu search, simulated annealing, and a whole host of others. Initially, four methods were developed directly within the GridLAB-D environment, namely a discrete optimizer,

continuous gradient descent, coordinated descent via Newton's method, and particle swarm optimization. However, it was quickly realized that developing all of these capabilities within the environment would not be cost effective, as there are a number of tools available for performing advanced optimization techniques (MATLAB®, MOSEK, CPLEX, etc.). Instead, a "link" tool was created within GridLAB-D that allows exchange of information with other pieces of software, particularly those that contain libraries of optimization solvers. Initial focus was on integrating with MATLAB. This allows users to pass information from within the GridLAB-D simulation into MATLAB, perform an optimization function (or any other operation), then pass the control variables back into the GridLAB-D environment and continue the simulation. By adding this feature, it allows users to greatly expand the library functions available in GridLAB-D without investing considerable resources in development. MATLAB was chosen over other tools because of the flexibility it allows over strictly optimization tools – MATLAB contains a number of other features that are useful to engineers working in the GridLAB-D environment, such as the Control System Toolbox and plotting functions. More information about the MATLAB link capabilities, and how to use the link, can be found at [12].

3.2 Implementation

To highlight the capabilities of the multi-objective controls, a battery storage model within the GridLAB-D environment was used. The storage and inverter models are complex enough to capture temperature dependent charging efficiencies, voltage dependencies, and parasitic consumptions. The controls were designed to maximize the revenue generated by charging and discharging the battery within different electricity markets, while minimizing the operational costs. This section will briefly describe this solution.

3.2.1 Optimization Strategies

Due to the limited amount of energy storage, the operation of battery in different time periods is interdependent. Providing more energy into the grid in one period increases the revenue for that period, but results in less energy able to be sold in following time periods, therefore (possibly) reducing the overall revenue. Hence, the battery operation for each time period needs to be carefully determined by solving a multi-period optimization problem based on the forecast information. For this analysis, optimization problems were developed to maximize the utility of an energy storage device for participation in a wholesale energy market and a ramping services market. It is assumed that the participation of such devices is on a small scale, such that it does not affect the market price. Three optimization strategies were evaluated to optimize the battery operation, based on different assumptions:

1) In the first strategy, it was assumed that the forecasted five-minute prices within the next 24 hours (or other fixed length time horizon) are available. Of course, in most market systems, only hourly prices are forecasted, but this is used as an example (and hourly prices could be assumed over the five-minute windows). The average price is used as an indicator for determining how much energy is to be charged or discharged within the next 24 hours. Based on this information, the current SOC of the battery at each five-minute time period,

and the desired SOC at the end of 24 hours, an optimized charge/discharge schedule can be created, and solved to determine the battery operation for the current period. Owners of the battery storage may repeat this optimization every period. In other words, a rolling window model is used to determine the optimal operation for the each period on five-minute basis. It should be noted that in each period, specifying a SOC at the end of each time horizon (24 hours in this case) does not aim to actually obtain the given SOC at that time, but merely to enable the optimization engine to make the best decision for current period based on the latest information. Figure 3.1(a) graphically illustrates the optimization time periods.

2) In the second strategy, it is assumed that hourly day-ahead electricity prices are available before the beginning of operating day. In addition, it was assumed that the hourly electricity prices can reflect the trend of five-minute prices. Therefore, the average day-ahead hourly energy price is used to determine how much energy will be charged or discharged during the operating day. Based on this information and SOC at the beginning of the day, one can specify the desired SOC at the end of the day. At each five-minute time period, the battery owner can formulate and solve an optimization problem over the time horizon from the current period to the end of the day, based on the five-minute prices. This optimization will be repeated each period through the operating day, with the same desired SOC at the end of the day, but over a gradually reduced time horizon. In each optimization, the specified SOC at the end of optimization time horizon (the end of day) remains the same. Figure 3.1(b) graphically illustrates the optimization time periods.

3) In the third strategy, it is assumed that the real-time prices can only be forecasted within a limited time frame that is less than 24 hours. Therefore, a day is divided into several time blocks so that the real-time price through each time block is available at the beginning the time block. Similar to the previous strategy, the day-ahead price information is used to set SOC at the end of each time block. At each period, the optimization problem can be formulated and solved over a time horizon from current period to the end of the time block, based on the forecast five-minute prices. Figure 3.1(c) graphically illustrates the optimization time periods.

No matter which strategy is selected, at each period, the same multi-period optimization problem is solved, but over a time horizon with different lengths. The next section will describe the mathematical formulation of the optimization problem.

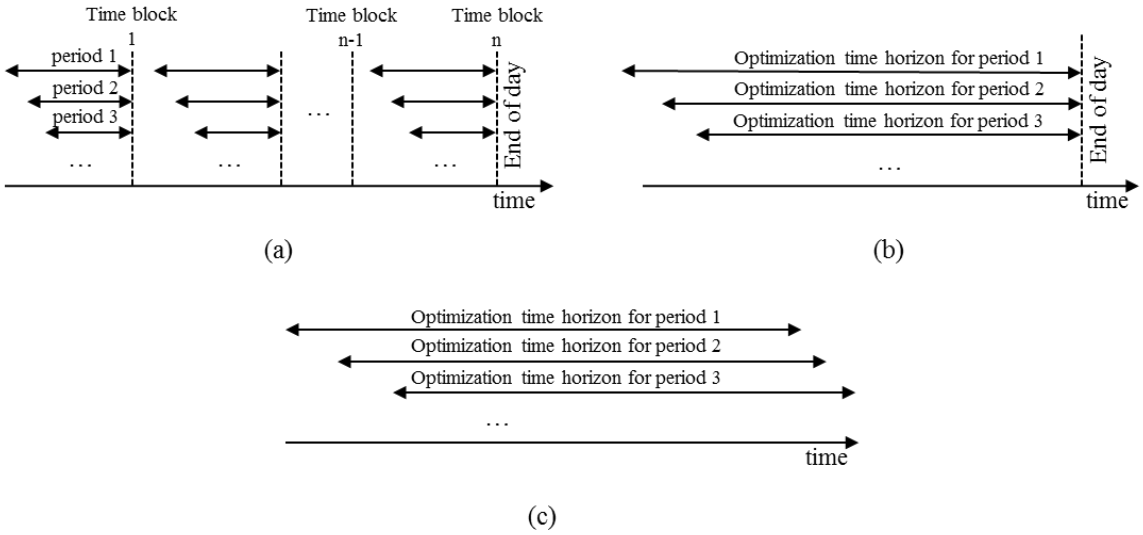

Figure 3.1: Time periods of optimization for each strategy

3.2.2 Mathematical Formulation of Optimization Problem

This section presents the mathematical formulation of the multi-period optimization problem to be solved in each period. Both deterministic and stochastic optimization models are presented.

3.2.2.1 Deterministic model (Revenue maximization)

The revenue is the total net income from both the wholesale energy and ramping service markets. Assuming λ_k and γ_k, representing the wholesale energy price and the ramping price of time period *k* respectively, can be forecasted within reasonable accuracy, and ignoring the associated uncertainty, the revenue maximization can be formulated as a deterministic optimization problem, as shown in equations (1a) to (1n).

$$\max_{p_k^+, p_k^-, p_k, p_k^{batt}, e_k, e_k^{batt}, l_k, h_k} \quad \sum_{k=1}^{K} (\lambda_k e_k + \gamma_k h_k) \tag{1a}$$

subject to:

Power injection limit:	$0 \le p_k^+ \le p_{\max}^+$	$\forall k = 1,\ldots,K$	(1b)
Power withdrawal limit:	$0 \le p_k^- \le p_{\max}^-$	$\forall k = 1,\ldots,K$	(1c)
Charging or Discharging only:	$p_k^+ p_k^- = 0$	$\forall k = 1,\ldots,K$	(1d)
Power transfer between battery and grid:	$p_k = p_k^+ + p_k^-$	$\forall k = 1,\ldots,K$	(1e)
Successive periods of charge/discharge not allowed::	$0 \le p_k p_{k-1}$	$\forall k = 1,\ldots,K$	(1f)

Rate of change of energy in battery:	$p_k^{batt} = \frac{p_k^+}{\eta^+} - p_k^- \eta^-$	$\forall k = 1,\ldots,K$	(1g)
Energy transfer between battery and grid:	$e_k = \frac{p_{k-1} + p_k}{2} \Delta T$	$\forall k = 1,\ldots,K$	(1h)
Change of energy in battery:	$e_k^{batt} = \frac{p_{k-1}^{batt} + p_k^{batt}}{2} \Delta T$	$\forall k = 1,\ldots,K$	(1i)
Ramping:	$p_k - p_{k-1} = h_k$	$\forall k = 1,\ldots,K$	(1j)
State of charge:	$l_k = l_{k-1} - \frac{1}{E_s} e_k^{batt}$	$\forall k = 1,\ldots,K$	(1k)
State of charge limits:	$l_{\min} \le l_k \le l_{\max}$	$\forall k = 1,\ldots,K$	(1l)
Ramping limits:	$r^{down} \le \frac{p_k - p_{k-1}}{\Delta T} \le r^{up}$	$\forall k = 1,\ldots,K$	(1m)
Desired SOC at end of time horizon:	$l_K = l_{set}$	$\forall k = 1,\ldots,K$	(1n)

The associated uncertainty will be dealt with in later sections. The updated forecast of λ_k and γ_k are used to solve this optimization problem during each time period *k*. Constraints (1b) and (1c) enforce the bounds of power injection and withdrawal by the battery to or from the grid, respectively. Constraint (1d) is nonlinear, which ensures charging and discharging does not take place at the same time. However, when battery efficiencies (including power electronics), η^+ or η^-, are considered as non-ideal and have a value less than 1 and λ_k is positive, this constraint is not necessary. Constraint (1e) describes the amount of power transfer between the battery and the grid, where p_k^+ is the amount of power injected into the grid during discharge, p_k^- is the power demand from the grid during charging, and p_k is the total power exchange with the grid where a positive number indicates the battery is discharging. Constraint (1f) ensures power does not cross zero within a period. This prevents over-cycling of the battery. Constraint (1g) expresses the rate of change of energy stored in the battery. Constraint (1h) calculates the energy, e_k, injected into (or withdrawn from) the grid using trapezoidal criterion, constraint (1i) calculates change of energy stored in battery using trapezoidal criterion, and constraint (1j) relates power and ramping capacity by assuming the actual ramping is always equal to the committed ramping capacity, h_k, and by assuming the power changes linearly from the beginning to the end of each period. Constraint (1k) calculates the SOC, l_k. Constraint (1l) restricts the battery charge level to be between its lower and upper bounds, $l_{\min}$ and $l_{\max}$, which for this application assumes the maximum and minimum *practical* ranges of the device. Constraint (1m) is the limit describing the maximum rate of change of power, or the ramping down, r^{down}, or up, r^{up}, limits per unit time. Constraint (1n) allows the user to specify the SOC,

l_{set}, at the end of the scheduled time horizon, l_K, so that the SOC can be guaranteed at a given time if desired by the user. It should be noted that p_1^+, p_1^-, and l_1 are the parameters of this optimization, which represent the initial conditions of battery at the beginning of the first period.

Modeling tricks can be used to replace (1f) with linear constraints, so that the problem can also be solved by mixed integer linear programming solvers. Since $p_{k-1}p_k \geq 0$ is equivalent to

$$\begin{cases} |p_{k-1}| \leq |p_{k-1} + p_k| & \text{(2a)} \\ |p_k| \leq |p_{k-1} + p_k| & \text{(2b)} \end{cases}$$

either

$$p_{k-1} + p_k \geq \max\{|p_{k-1}|, |p_k|\} \tag{3}$$

or

$$-p_{k-1} - p_k \geq \max\{|p_{k-1}|, |p_k|\} \tag{4}$$

must be true. The Big-M method can be used to reformulate above in equations as linear constraints [13]:

$$p_{k-1} \leq z_k \tag{5a}$$

$$-p_{k-1} \leq z_k \tag{5b}$$

$$p_k \leq z_k \tag{5c}$$

$$-p_k \leq z_k \tag{5d}$$

$$-p_{k-1} - p_k \leq -z_k + M s_k^+ \tag{5e}$$

$$p_{k-1} + p_k \leq -z_k + M s_k^- \tag{5f}$$

$$s_k^- + s_k^+ = 1 \tag{5g}$$

where M is a constant whose value is set to be sufficiently large so that the constraint $-p_{k-1} - p_k \leq -z_k + M$ or $p_{k-1} + p_k \leq -z_k + M$ can be ignored, z_k is a free variable, and s_k^-, s_k^+ are binary.

3.2.2.2 Deterministic model (Profit maximization)

The cost of battery storage includes both capital investment and operational costs. The operational costs may include maintenance, labor, etc., that can be assumed to be independent of the operation of battery storage, i.e., whether the battery is used a lot or very little, maintenance requirements will still be fairly similar. The investment cost depends on the battery type and capacity in terms of both MWh and MW, but does not vary with the operation of battery. However, the operational strategy of the battery affects the lifetime of the battery, and therefore must be considered when determining the total amount of energy traded.

Cycle life is the most commonly quoted measure of battery life. It is usually defined as the number of cycles completed before capacity falls to less than 80% of the rated capacity under constant controlled environments and operating conditions with specific temperature and depth-of-discharge (DOD) [14]. *Life energy throughput* is a more representative measure of battery life, which is the total amount of energy that can be put into and taken out of a battery over all the cycles before its capacity reduces to 80% of its initial capacity. The life throughput energy, L_E, is expressed as in [15][16]:

$$L_E = L_C E_S D \tag{6}$$

where L_c is the cycle life, E_s is the battery energy capacity, and D is the DOD for which L_c is determined. Many factors affect cycle life and therefore life throughput energy, such as DOD, discharge rate, ambient temperature, charging regime, battery maintenance procedures [14][17]. In order to maintain certain battery life throughput energy, battery owners may choose to stop discharging battery when SOC is below certain point; they may also choose to continue discharging the battery if the electricity price is high enough to cover the cost associated with loss of battery life due to a deep discharge. Assuming the temperature is controlled for optimal battery life and excluding it from decision variables, then the associated cost of battery aging for a certain operation in a period is given as a function of l_k, l_{k+1}, p_k, p_{k+1}, and e_k^{batt}, i.e., $f(l_k, l_{k+1}, p_k, p_{k+1}, e_k^{batt})$, and the profit over the scheduled time horizon can be expressed as

$$\max \sum_{k=1}^{K} \left[\lambda_k e_k + \gamma_k h_k - f\left(l_k, l_{k+1}, p_k, p_{k+1}, e_k^{batt}\right) \right] \tag{7}$$

which can be used to replace (1a) to maximize the profit. However, the determination of the battery life is very difficult because it is based on lab tests and experimentation. Large numbers of batteries must be tested to determine battery cycle life under a few constant operational conditions, which is costly and may also require a long test period. For a battery storage device that is operated under a wide variety of operating conditions, cycle life at a few specific DOD points does not provide a full picture as the battery is not cycling from full capacity to the specific DOD all of the time. On the other hand, it is impossible to test batteries under all

operational conditions. Therefore, it is very difficult to obtain a function that quantifies the associated cost of a certain charging or discharging operation within a period. Due to these reasons, when optimizing the battery operation, it is not uncommon to assume the cost associated with loss of battery life is independent of operation of battery [18]–[20].

When $f(\cdot)$ becomes constant, it can be excluded from (7). Under this assumption, the solution for revenue maximization also yields the maximum profit. In this approach, rather than using a constant daily battery cost, it is assumed that the life throughput energy is constant. Therefore, one can estimate the cost associated with charging and discharging, denoted by α. The cost, *f*, can be expressed as a function of e_k^{batt}:

$$f\left(e_k^{batt}\right) = \alpha\, e_k^{batt}, \qquad when\ e_k^{batt} > 0 \tag{8}$$

Again, tricks can be played to replace this nonlinear constraint with linear ones:

$$f\left(e_k^{batt}\right) = \alpha\left(e_k^{batt} + y_k\right)/2 \tag{9a}$$

$$y_k \geq e_k^{batt} \tag{9b}$$

$$y_k \geq -e_k^{batt} \tag{9c}$$

where y_k is again a free variable. An alternative method to (9) is:

$$f\left(e_k^{batt}\right) = \alpha \frac{p_{k-1}^{+} + p_k}{2\eta^{+}} \Delta T \tag{10}$$

which has the advantage over (9) because no additional decision variables are introduced.

3.2.2.3 Stochastic programming or robust optimization

Different methods can be used to model the uncertainties associated with λ_k and γ_k, and techniques such as stochastic programming and robust optimization can be used to formulate and solve this problem. Updated forecast information for λ_k and γ_k, whether the exact probability density function (PDF) or the range of the prices, are used to solve the linear program within each update period.

If the prices are formulated as random variables and the PDF is provided, one strategy is to maximize the expected revenue. The objective function becomes

$$\max_{p_k, e_k, l_k, h_k} \left(\lambda_1 e_1 + \gamma_1 h_1 + \int_V R(v) f(v) dv\right) \tag{11}$$

where V denotes the domain of ν, and $f(v)$ is the PDF of ν. If the uncertainty is modeled using certainty intervals for λ_k and α_k, the robust model can be formulated using the method in [21]. If λ_k and α_k represent the degree of importance of the energy and ramping capacity rather than price, i.e., the user specifies the relative importance of the two services, the objective value can be found that maximizes the minimum for a considered range of λ_k and α_k, i.e.,

$$\max_{p_k, e_k, l_k, h_k} \left[\min_{\lambda_k, \gamma_k} \left(\lambda_1 e_1 + \gamma_1 h_1 + \sum_{k=2}^{K} \left(\lambda_k e_k + \gamma_k h_k \right) \right) \right] \tag{12}$$

3.2.3 Simulation Results

In this section, the operation of a 500 kW DPR™ [22] is optimized using the second strategy described in Section 3.2.1 and the deterministic revenue maximization approached discussed in Section 3.2.2.1. The assumed parameters of the battery storage device are given in Table 3.1 and simulated within the GridLAB-D environment using these parameters. The designated time period between optimization updates is five minutes. The output power and SOC at the beginning of the first period are assumed be zero and 50%, respectively. Since real-time price data of energy and ramping services from distributed battery storage devices are not available, in this study, the historical data for five-minute Locational Marginal Price (LMP) at a node within the real-time market of Midwest ISO (MISO) is used to represent α_k [23]. The ramping capacity prices, γ_k, were created by using the difference between settled MW in the current period and the next period in the real-time MISO market. GLPKMEX [24] for MATLAB is used to solve the optimization problem formulated in (1), with (1f) replaced by (5). Cases that were studied are listed in Table 3.2. It should be noted that for all of the cases except Case 3 the forecast price uncertainty is not included, so the results from running one optimization at the beginning of the day or repeating the optimization every period through a day are the same.

Table 3.1: Parameters of implemented 500 kW lead-acid battery

Parameter	Value	Parameter	Value
$P^{+}_{\max}$	500 kW	$P^{-}_{\max}$	500 kW
$l_{\min}$	0%	$l_{\max}$	100%
η^{+}	0.85	η^{-}	0.85
r^{up}	180 MW/h	r^{down}	180 MW/h
E_s	3 MWh	ΔT	5 min.

Table 3.2: Description of test cases

	Optimization Objective	I_K	λ_k contains hour-of-day component	Forecast Price Uncertainty
Case 1.1	$\sum_{k=1}^{K} \lambda_k e_k$	(1n) is not enforced	No	No
Case 1.2	$\sum_{k=1}^{K} \lambda_k e_k$	0.5	No	No
Case 1.3	$\sum_{k=1}^{K} \lambda_k e_k$	0.5	Yes	No
Case 1.4	$\sum_{k=1}^{K} \left[\lambda_k e_k - \alpha\left(e_k^{batt} + y_k\right)/2\right]$	0.5	Yes	No
Case 2	$\sum_{k=1}^{K} \left[\lambda_k e_k + \gamma_k h_k - \alpha\left(e_k^{batt} + y_k\right)/2\right]$	0.5	Yes	No
Case 3	$\sum_{k=1}^{K} \left[\lambda_k e_k + \gamma_k h_k - \alpha\left(e_k^{batt} + y_k\right)/2\right]$	0.5	Yes	Yes

3.2.3.1 Case 1: Single Objective

In this first test case, the revenue from the ramping services is excluded for illustration and simplicity purposes. This is used to demonstrate the optimization methods on a single source of revenue before applying it to multiple objectives.

Case 1.1: Constraint (1n) is not enforced. The assumed energy price together with the resulted optimal power transfer between the battery and grid are shown in Figure 3.2. The revenue is $76.1 under the assumed electricity price. The SOC of battery is shown in Figure 3.3. As expected, without constraint (1n), revenue within the current scheduling time horizon is maximized by fully discharging the battery at the end of the horizon. However, over long term (e.g., a month), the net change of energy in battery should be zero.

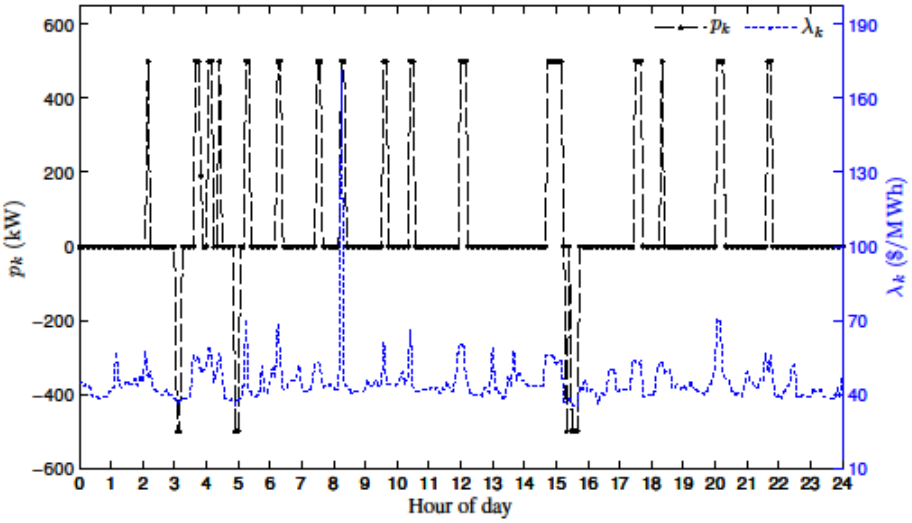

Figure 3.2: Power exchange (p_k) and price (λ_k) over 24 hour period for Case 1.1

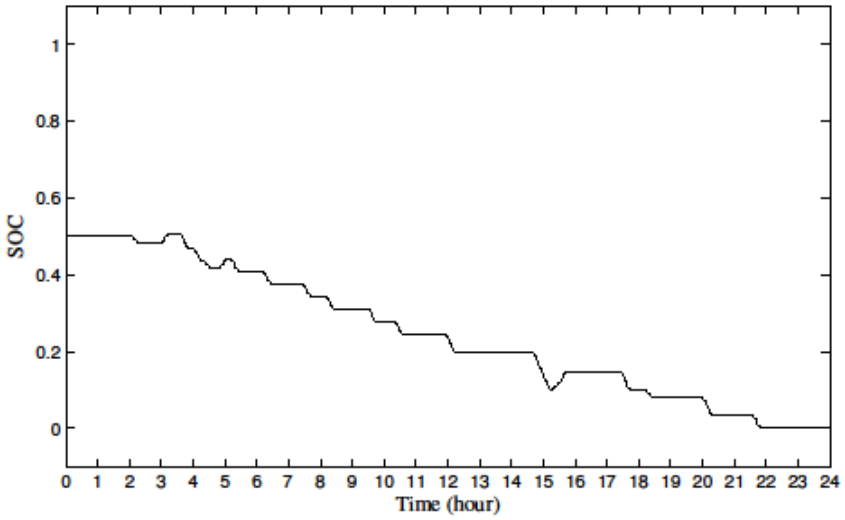

Figure 3.3: Battery SOC over 24 hour period for Case 1.1

Case 1.2: In this case and each of the following cases, constraint (1n) is enforced. The second strategy, as discussed in Section 3.2.1, is used so that the amount of energy charged or discharged during the operating day is determined based on the day-ahead electricity price. Using this information together with the initial SOC at beginning of the day (l_o), l_K is can be calculated. In this example, l_K is assumed to be given and equal to 0.5. The corresponding power transfer between battery and grid and battery SOC are plotted again in Figure 3.4 and Figure 3.5, respectively. The resulted maximum revenue is $8.60. As can be seen, the battery SOC does not vary much through the time horizon. This is because the 5-minute real-time energy price is quite random, and there are no peak and off-peak periods. Therefore, revenue will not increase by injecting or withdrawing electricity from/to grid over a relative long period (e.g., several hours). For this particular pattern of electricity price, the energy capacity is oversized relative to its rated power.

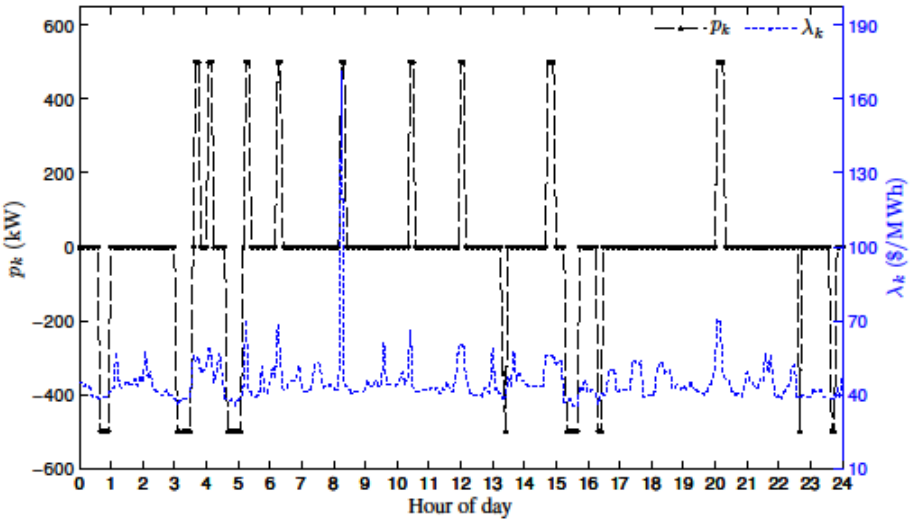

Figure 3.4: Power exchange (p_k) and price (λ_k) over 24 hour period for Case 1.2

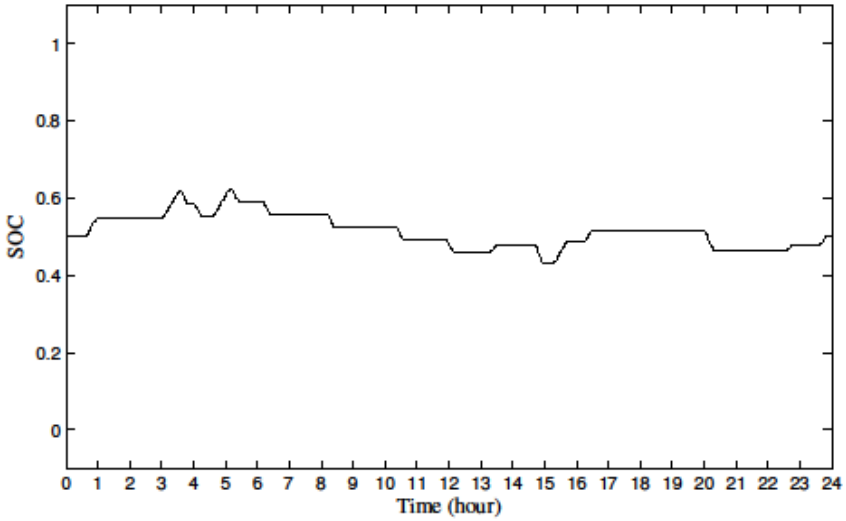

Figure 3.5: Battery SOC over 24 hour period for Case 1.2

Case 1.3: If the energy price also contains low frequency component (varying from peak to off-peak hours) in addition to high frequency component (changing from one 5-minute to another), the charge and discharge pattern will be very different. Figure 3.6 and Figure 3.7 plot the power transfer between battery and grid and battery SOC, for the price shown in Figure 3.6. The corresponding maximum revenue is $58.10. For this price pattern, the battery is generally charged during off-peak hours and discharged during peak hours. It should be noted that the battery could also switch between charging and discharging within peak or off-peak hours, depending on the battery energy to power ratio and price signal. For example, reducing the battery energy size to 1 MWh, the power and battery SOC are plotted again in Figure 3.8 and

Figure 3.9. The corresponding maximum revenue is $34.20. For a given price pattern, the energy to power ratio could be a treatment factor, based on which the battery size can be optimized.

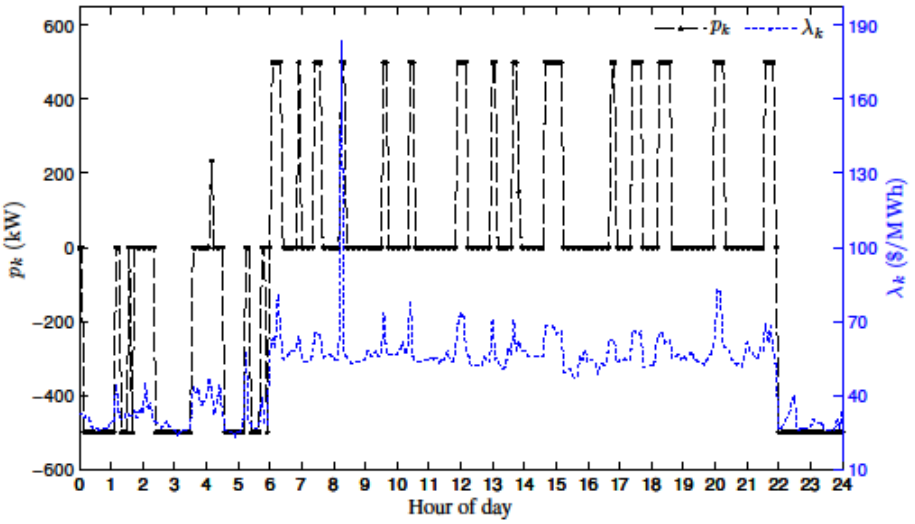

Figure 3.6: Power exchange (p_k) and price (λ_k) over 24 hour period for Case 1.3

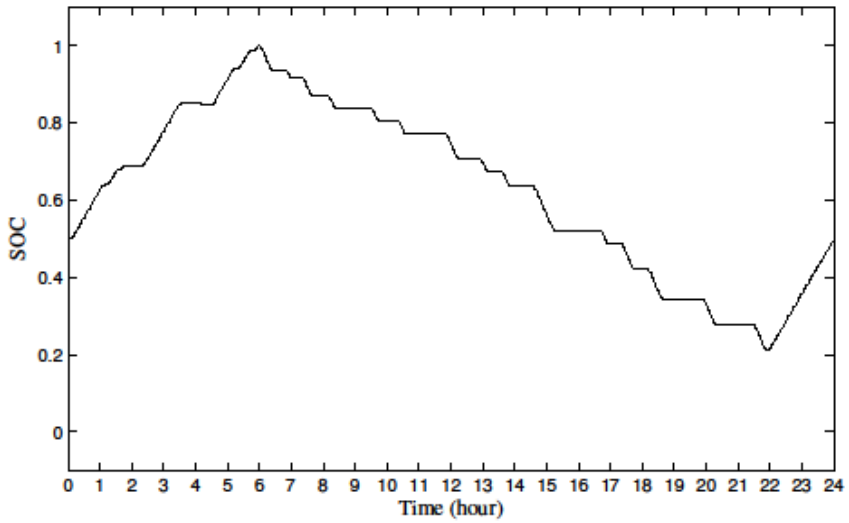

Figure 3.7: Battery SOC over 24 hour period for Case 1.3

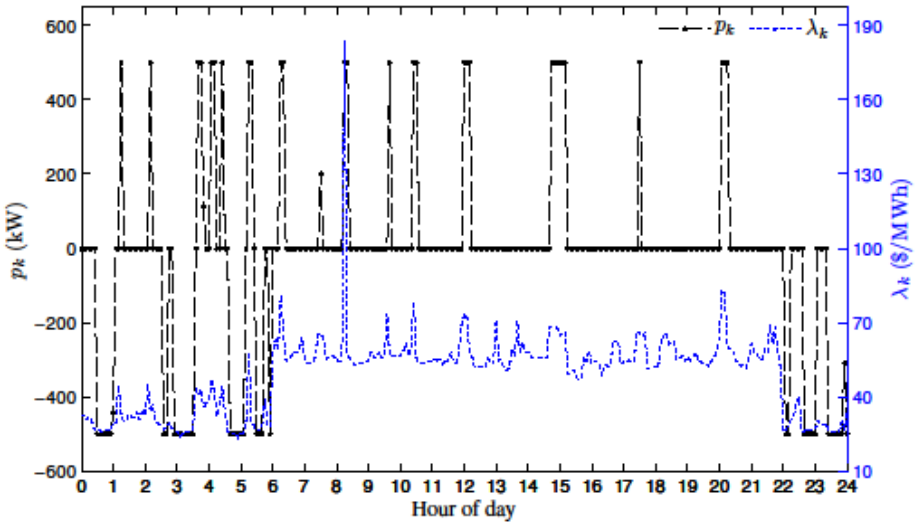

Figure 3.8: Power exchange (p_k) and price (λ_k) over 24 hour period for Case 1.3 with $E_s = 1$

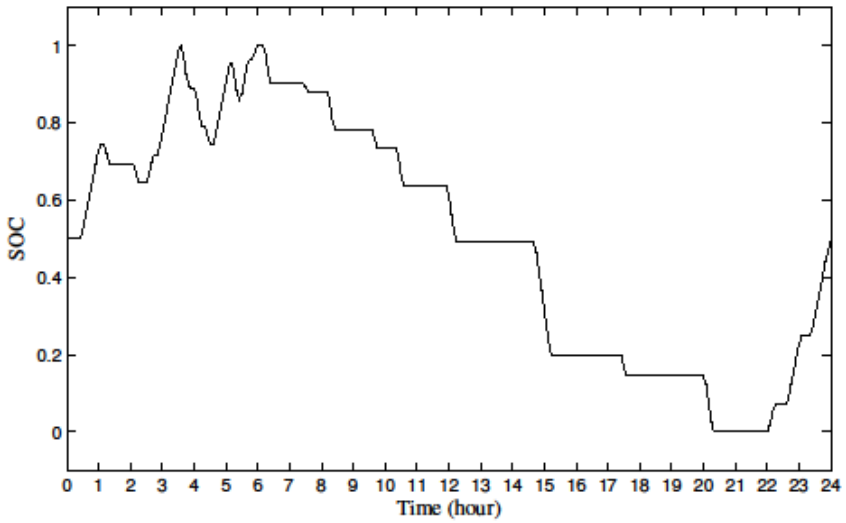

Figure 3.9: Battery SOC over 24 hour period for Case 1.3 with $E_s = 1$

Case 1.4: In this case, the battery cost is included into the objective function using the method described in (10). The cost and cycle life information for different battery technologies (e.g., lead-acid, sodium-sulfur, and lithium-ion) can be found in [25]–[27]. Under today's technology, the average cost per unit energy throughput over the battery lifespan is generally higher than $50/MWh. When assuming $\alpha = 50$, the power and battery SOC are shown in Figure 3.10 and Figure 3.11, respectively. As can be seen, there is almost no energy transfer between battery and grid, because under the assumed energy price, revenue from energy trading cannot compensate the cycling cost. When α is reduced to 20, the results are shown in Figure 3.12 and Figure 3.13. The maximum profit and the corresponding revenue are $14.00 and $47.40, respectively.

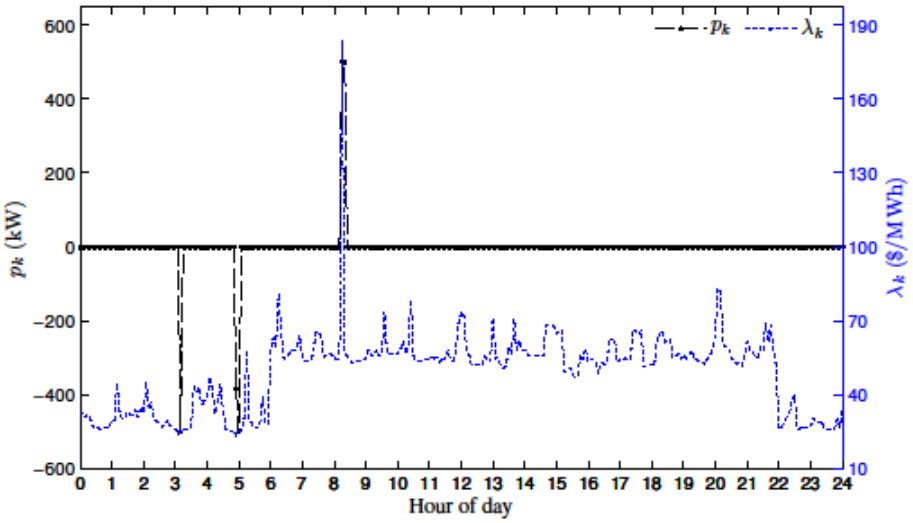

Figure 3.10: Power exchange (p_k) and price (λ_k) over 24 hour period for Case 1.4 with α = 50

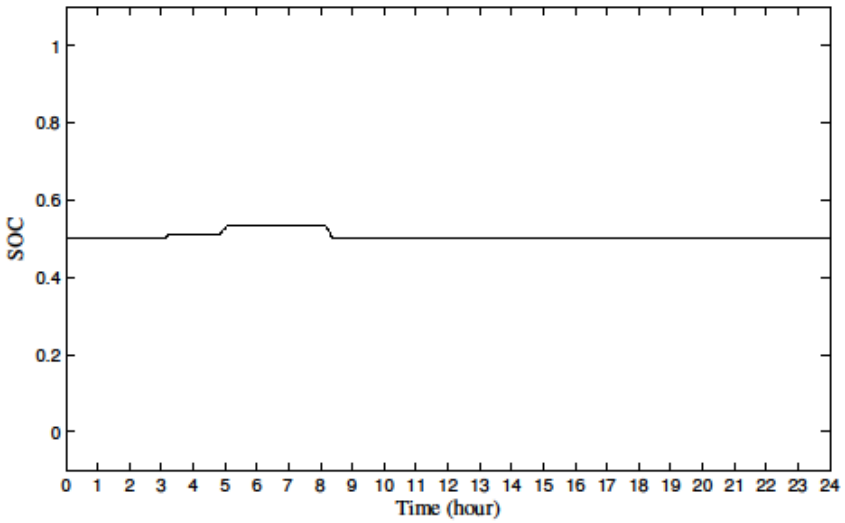

Figure 3.11: Battery SOC over 24 hour period for Case 1.4 with α = 50

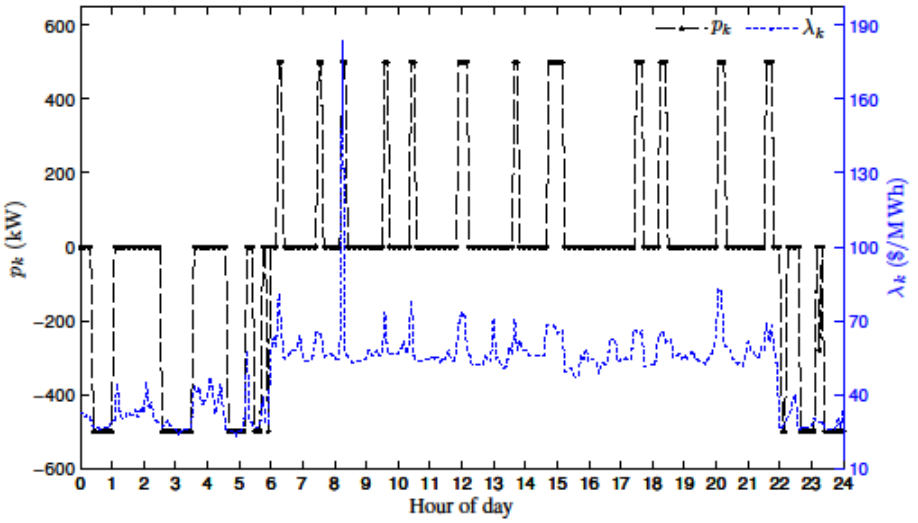

Figure 3.12: Power exchange (p_k) and price (λ_k) over 24 hour period for Case 1.4 with α = 20

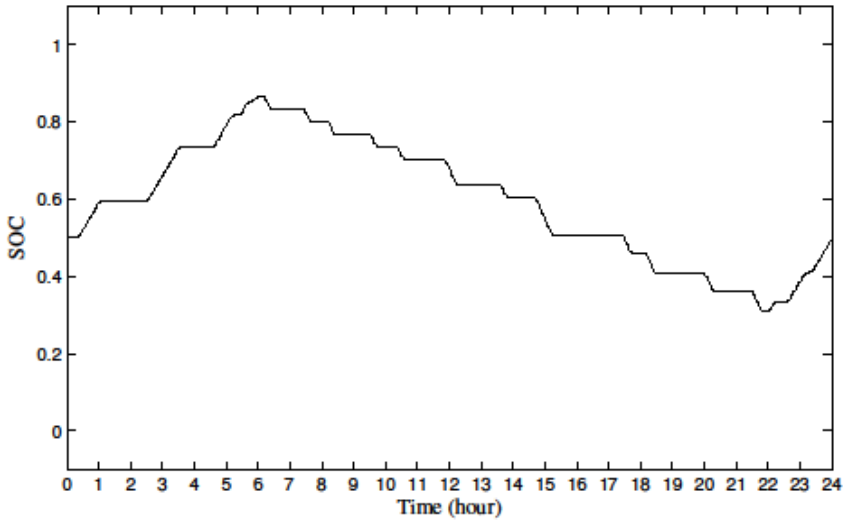

Figure 3.13: Battery SOC over 24 hour period for Case 1.4 with α = 20

3.2.3.2 Case 2: Dual-Objective

In this case, energy trading, ramping service and battery cost are all included in the objective function. The difference between this case and Case 1.4 with α = 20 is the inclusion of ramping service. The assumed energy and ramping capacity prices are shown in Figure 3.14. The resulted optimal scheduling of power transfer between battery and grid is shown in Figure 3.15. The maximum profit and corresponding revenue are $39.50 and $80.70, respectively. Due to the ramping service component, the battery is charged and discharged more frequently than Case 1.4 (Figure 3.12). Furthermore, the addition of revenue from ramping service can help to cover the battery cycling cost, and therefore tends to increase the amount of energy exchange between battery and grid. This is why the SOC in Figure 3.16 varies more than Figure 3.13.

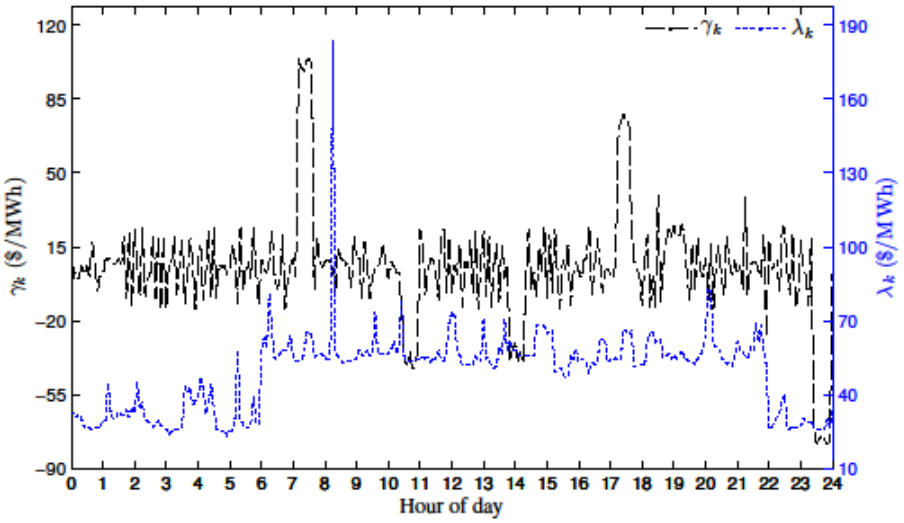

Figure 3.14: Energy price (λ_k) and ramp rate price (γ_k) over 24 hour period for Case 2

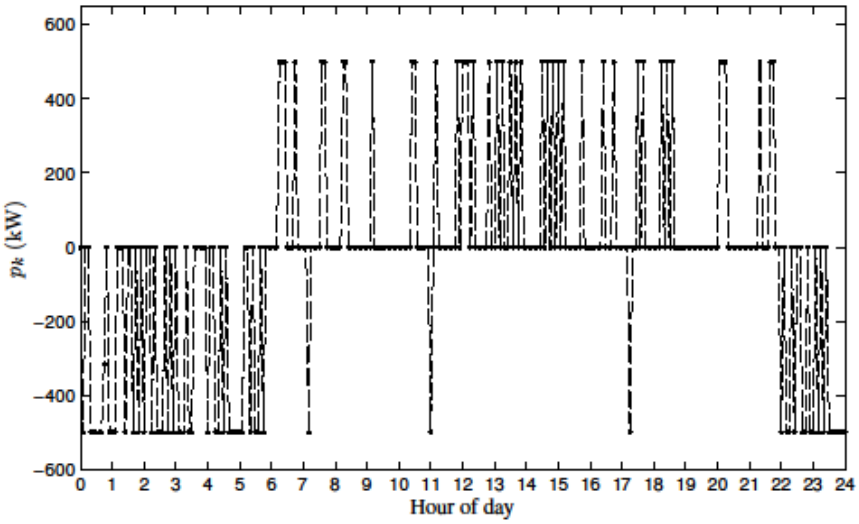

Figure 3.15: Power exchange (p_k) over 24 hour period for Case 2

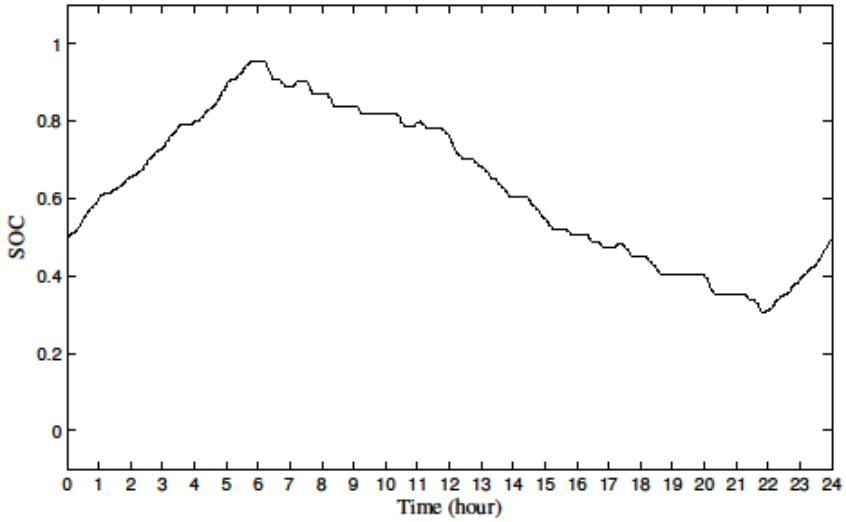

Figure 3.16: Battery SOC over 24 hour period for Case 2

3.2.3.3 Case 3: Dual-Objective with Price Forecast Error

The actual prices used in this case are the same as used in Case 2. However, the forecast price is not assumed to be perfect anymore—a forecast error is introduced based on simple rules. For example, the forecast price for each period can be modeled as the sum of the actual price and a Gaussian error term, $P_i^{forecast} = P_i + N(0,\sigma)$, where P_i represents either energy price or ramping capacity price. When the generated energy price becomes negative (only limited number of periods), zero is used. Nevertheless, this adjustment does not significantly affect the results when σ is small compared with the actual price. This simplified assumption is not based on realistic forecast model, but only used to illustrate how the forecast error could affect the profit, as the focus of this study is the optimization formulation rather than the price forecast techniques and their performance. More realistic forecast error corresponding to different forecast techniques could be used in future work. For σ = \$10/MWh and σ = \$20/MWh, the maximum profit and corresponding revenue are shown in Table 3.3, which also contains the results of Case 2 for convenience. As expected, the profit decreases when forecast error increases.

Table 3.3: Profit and revenue from energy and ramping services with difference forecast error

	Case 2 (perfect forecast)	Case 3 (with forecast error)	
		σ = \$10/MWh	σ = \$20/MWh
Profit	\$ 39.50	\$ 33.20	\$ 12.70
Revenue	\$ 80.70	\$ 72.90	\$ 56.10

3.3 Test Case using Modified DECC Facility Model

As a way to show how multi-objective controls could be used and evaluated in a simulation environment, a test model using the modified DECC model discussed in Section 2.3.2 was created. The modified DECC model was again modified to add a 50 kW, 300 kWh at node 10 as shown in Figure 3.17. Additionally, the static loads were replaced with time-series load shapes representative of commercial buildings. The model was simulated in GridLAB-D over a 24 hour period, using the MATLAB optimization tool as described in Section 3.2.3.2 with the settings shown in Table 3.4.

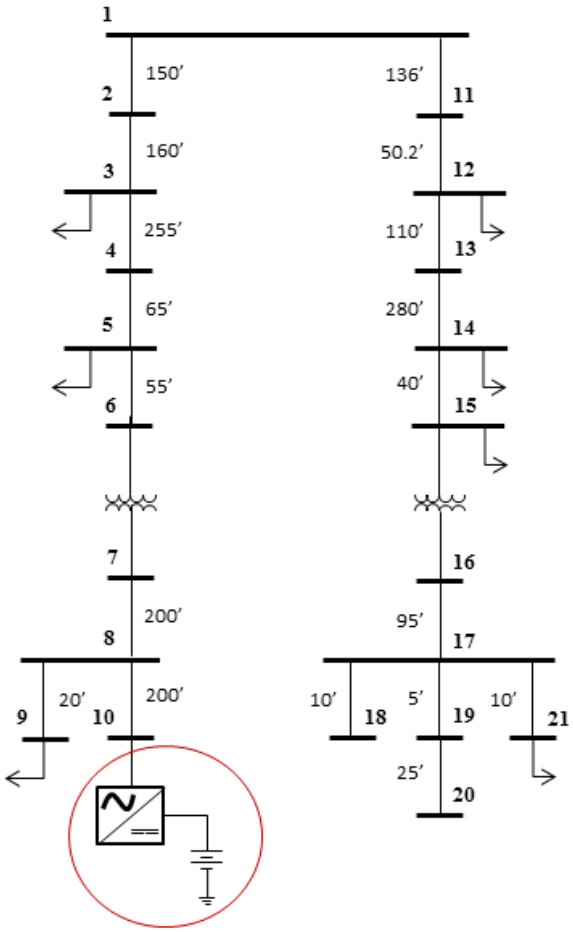

Figure 3.17: Modified DECC facility model with energy storage added

Table 3.4: Parameters of implemented DECC battery storage case

Parameter	Value	Parameter	Value
$P^{+}_{\max}$	50 kW	$P^{-}_{\max}$	50 kW
$l_{\min}$	0%	$l_{\max}$	100%
η^{+}	0.8	η^{-}	0.8
r^{up}	50 kW/h	r^{down}	50 kW/h
E_s	300 kWh	ΔT	5 min.
l_o	0.5	l_K	0.5

For simplicity, and to show how the battery optimization might be used in a (at times) isolated micro grid, the energy price signal, λ_k, was created using a linear relationship with the base load shape, i.e., as load demand, so did price. The ramping price signal, γ_k, was generated by taking the derivative of the energy price as a function of time. The prices used are shown in Figure 3.18. While this price signal is not necessarily realistic in terms of dollars, nor is this control ideal for all situations, it highlights how the control optimization tool can be used on an integrated simulator to evaluate the performance of a control system.

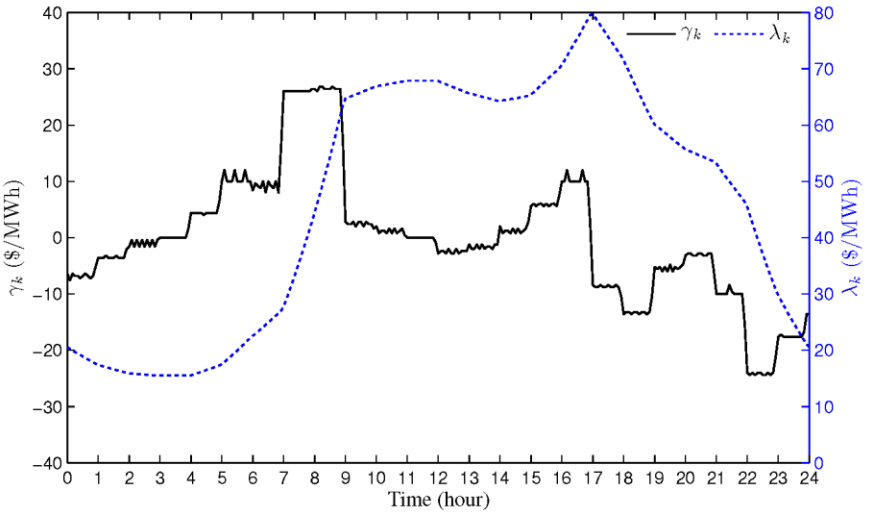

Figure 3.18: Price signals for DECC example

Figure 3.19 shows the time-series substation load (kW) from the simulated system, both with and without the battery storage device. Figure 3.20 shows the time-series battery output (kW). Note that because the "price" was a function of the total demand, it had the effect of reducing the system peak by approximately 10%, while charging the battery during off-peak periods. Figure 3.21 shows the battery SOC during the 24 hour period. Note that the "predicted" model, which represents the MATLAB optimization model and what it is using to predict the next SOC will be, and the GridLAB-D model are not in perfect agreement. This is due to the fact that the GridLAB-D model is much more complicated than the optimization model, including voltage factors, weather related adjustments, and internal resistance models to calculate the actual

amount of load delivered (or withdrawn from) the battery at any given time. The MATLAB optimization model corrects at each time step, so that the models do not diverge. While in this case, the divergence of the optimization model and the "real system" are not significant, this does highlight some of the integrated test and design simulation environment. This gives users the ability evaluate control and optimization performance on a more realistic system via simulation rather than testing through actual deployment.

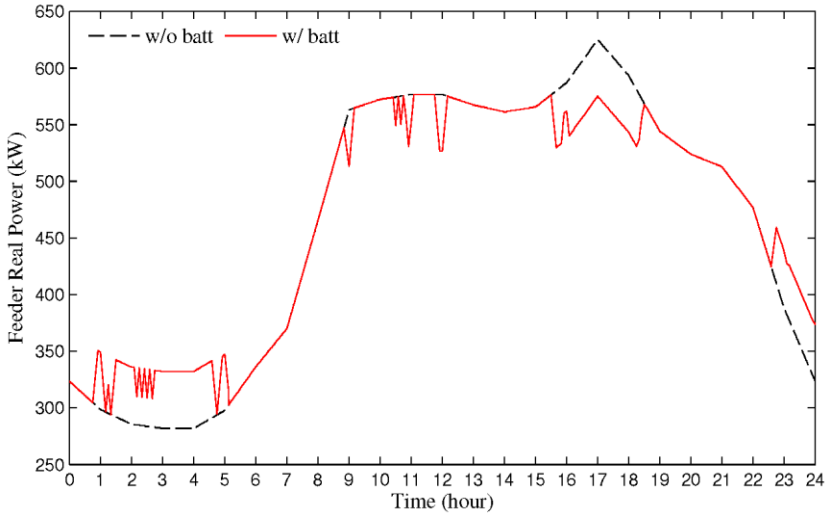

Figure 3.19: DECC feeder load shape with and without battery storage

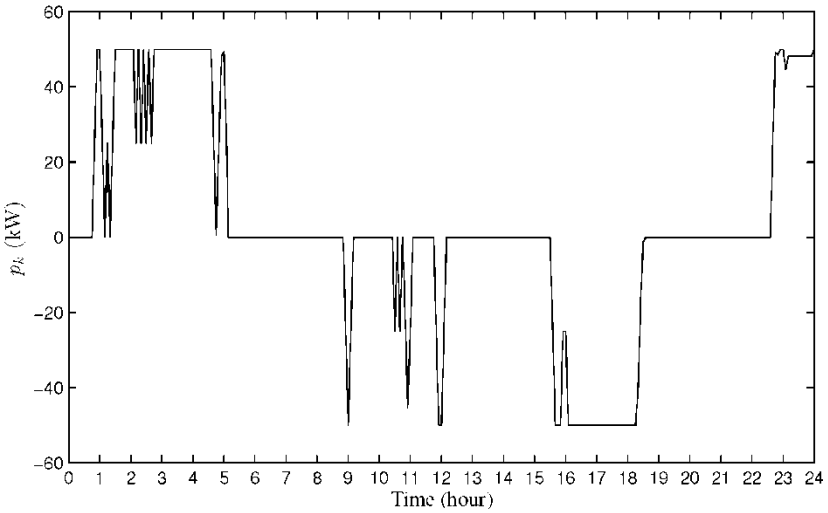

Figure 3.20: DECC model battery charge and discharge

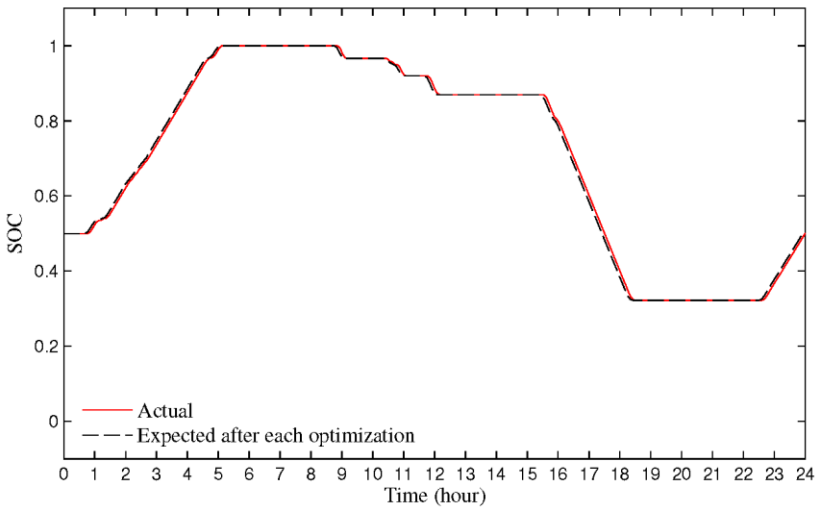

Figure 3.21: DECC model battery state of charge

4 Concluding Comments

As part of the Department of Energy's Office of Electricity Delivery and Energy Reliability Smart Grid and Micro Grid Research Programs, Pacific Northwest National Laboratory is continually developing next generation capabilities to facilitate the modernization of nation's electricity infrastructure. In FY12 this work focused on building new capabilities for the simulation and analysis of micro grids, and an open-source framework for the control and optimization of distributed resources. These two new capabilities will form the foundation for FY13 work that will focus on integrating, and expanding, these new capabilities with work conducted at Oak Ridge National Laboratory, Sandia National Laboratories, Lawrence Berkley National Laboratory, and Washington State University.

References

[1] T-H. Chen, M-S. Chen, T. Inoue, P. Kotas, and E. A. Chebli, "Three-phase cogenerator and transformer models for distribution system analysis," *IEEE Transactions on Power Delivery*, vol. 6, no. 4, 1991, 1671-1681.

[2] R. G. Harley, E. B. Makram, and E. G. Duran, "The effects of unbalanced networks on synchronous and asynchronous machine transient stability," *Electric Power Systems Research*, vol. 13, no. 2, 1987, 119-127.

[3] R. H. Salim and R. A. Ramos, "A Model-Based Approach for Small-Signal Stability Assessment of Unbalanced Power Systems," *IEEE Transactions on Power Systems*, vol.27, no.4, pp.2006-2014, Nov. 2012

[4] P. A. N. Garcia, J. L. R. Pereira, S. Carneiro, Jr., V. M. de Costa, and N. Martins, "Three-phase power flow calculations using the current injection method," *IEEE Transactions on Power Systems*, vol. 15, no. 2, 2000, pp. 508-514.

[5] P. Kundur, *Power System Stability and Control*, McGraw-Hill, New York, NY, 1994.

[6] E. B. Makram, V. O. Zambrano, and R. G. Harley, "Synchronous generator stability due to multiple faults on unbalanced systems," *Electric Power Systems Research*, vol. 15, no. 1, 1988, pp. 31-39.

[7] E. B. Makram, V. O. Zambrano, R. G. Harley, and J. C. Balda, "Three-phase modeling for transient stability of large scale unbalanced distribution systems," *IEEE Transactions on Power Systems*, vol. 4, no. 2, 1989, pp. 487-493.

[8] P. Krause, O. Wasynczuk, and S. Scott, "Analysis of electric machinery," *IEEE Power Engineering Society Magazine*, vol. 15, no. 3, 1995.

[9] P. Kundur and P. L. Dandeno, "Implementation of advanced generator models into power system stability programs," *IEEE Transactions on Power Apparatus and Systems*, vol. 7, 1983, pp. 2047-2054.

[10] GridLAB-D Contributors, "Dev:Microgrids", [Online]. Available: http://www.sourceforge.net/apps/mediawiki/gridlab-d/index.php?title=Dev:Microgrids. Accessed December 14, 2012.

[11] GridLAB-D Contributors, GridLAB-D, [Online]. Available: http://www.gridlabd.org. Accessed December 14, 2012.

[12] GridLAB-D Contributors, "Matlab link", [Online]. Available: http://sourceforge.net/apps/mediawiki/gridlab-d/index.php?title=Matlab_link.

[13] Griva, Igor, Stephen G. Nash, and Ariela Sofer. *Linear and nonlinear optimization*. Society for Industrial Mathematics, 2009.

[14] Battery and energy technologies. [Online]. Available: http://www.mpoweruk.com/index.htm

[15] W. Kempton and J. Tomić, "Vehicle-to-grid power fundamentals: Calculating capacity and net revenue," *J. Power Sources*, vol. 144, no. 1, pp. 268-279, Jun. 2005.

[16] C. Zhou, K. Qian, M. Allan, and W. Zhou, "Modeling of the cost of EV battery wear due to V2G application in power systems," IEEE Trans. Energy Convers., vol. 26, no. 4, pp. 1041–1050, Dec. 2011.
[17] S. Drouilhet and B. L. Johnson, "A battery life prediction methodfor hybrid power applications," in Proc. 35th AIAA Aerosp. Sci. Meet. Exhib., Reno, NV, Jan. 1997.
[18] A. K. Barnes, J. C. Balda, S. O. Geurin, and A. Escobar-Mejia, "Optimal battery chemistry, capacity selection, charge/discharge schedule, and lifetime of energy storage under time-of-use pricing," in Proc. IEEE Innovative Smart Grid Tech. (ISGT), Dec. 2011.
[19] H. Taheri, H. Ghasemi, A. Rahimi-Kian, and T. Akbari, "Modeling and optimized scheduling of virtual power plant," in Proc. Electrical Engineering (ICEE), May 2011.
[20] X. Zhang, R. Sharma, and Y. He, "Optimal energy management of a rural microgrid system using multi-objective optimization," in Proc. IEEE Innovative Smart Grid Tech. (ISGT), Jan. 2012.
[21] A. J. Conejo, J. M. Morales, and L. Baringo, "Real-time demand response model," IEEE Trans. Smart Grid, vol. 1, no. 3, pp. 236–242, Dec. 2010.
[22] "Xtreme Power". [Online]. Available: http://www.xtremepower.com/xp-technology/dpr-sizes.php. Accessed June 2012.
[23] Midwest Independent System Operator, "Markets and Operations", [Online]. Available: https://www.midwestiso.org/MarketsOperations/Pages/MarketsOperations.aspx
[24] "GLPKMEX." [Online]. Available: https://sourceforge.net/projects/glpkmex/
[25] E. Spahi´c and G. Balzer, "The application of batteries as a backup of large wind farms," presented at the 6th Conf. Large Scale Integr. Wind Power Trans. Sys. Offshore Wind Farms, Delft, Neth., Oct. 2006.
[26] P. Sullivan, W. Short, and N. Blair, "Modeling the benefits ofvstorage technologies to wind power," presented at the AWEA WindPower Conf., Houston, TX, Jun. 2008. [Online]. Available: http://www.nrel.gov/docs/fy08osti/43510.pdf
[27] Electricity Storage Association (ESA). [Online]. Available: http://www.electricitystorage.org/ESA/technologies/

Pacific Northwest
NATIONAL LABORATORY

Proudly Operated by **Battelle** *Since 1965*

U.S. DEPARTMENT OF
ENERGY

902 Battelle Boulevard
P.O. Box 999
Richland, WA 99352
1-888-375-PNNL (7665)
www.pnnl.gov